Available online at www.sciencedirect.com
SCIENCE DIRECT®
Solid State Ionics 161 (2003) 67–79
SOLID STATE IONICS
www.elsevier.com/locate/ssi

Grain boundary ionic conductivity of yttrium stabilized zirconia as a function of silica content and grain size

Michael C. Martin, Martha L. Mecartney*

National Fuel Cell Research Center (NFCRC), University of California, Irvine, CA, USA
Department of Chemical Engineering and Materials Science, 916 Engineering Tower, Irvine, CA 92697-2575, USA

Received 28 November 2002; received in revised form 2 April 2003; accepted 11 June 2003

Abstract

Impedance spectroscopy at temperatures from 350 to 700 °C and analytical electron microscopy were used to characterize grain boundary conductivity and grain boundary segregation of SiO_2 in 8 mol% yttrium stabilized zirconia (Y-CSZ). Colloidal silica in the amount of 1–10 wt.% (2.5–25 vol.%) was added as an intergranular phase. Various grain sizes were produced by sintering or annealing at temperatures of 1350–1600 °C for times from 0.1 to 100 h. The addition of intergranular SiO_2 led to decreased grain size (due to grain boundary pinning), increased grain boundary volume, and reduced total ionic conductivity. An increase in grain boundary width, from approximately 4 to 8 nm, was correlated with higher temperature anneal treatments and greater amounts of SiO_2. High temperature anneals of samples with silica reduced the grain boundary volume fraction by increasing the grain size and restored much of the total conductivity lost by adding silica. The grain boundary specific conductivity and the total ionic conductivity were not significantly affected by SiO_2 additions less than 5 wt.% when samples of a similar grain size were compared. This led to the conclusion that limited use of intergranular additives to create superplastic Y-CSZ should not degrade the ionic conductivity for a specific engineered grain size.

PACS: 66.30.D
Keywords: Grain boundary; Ionic conductivity; Stabilized zirconia; Grain size

1. Introduction

1.1. Background

Bauerle's [1] application of impedance spectroscopy to stabilized zirconia provided an analytical technique to determine the ionic conductivity of the grain interior and grain boundary of polycrystalline materials. Since that time, impedance spectroscopy has been used extensively to study ionic transport across the grain boundary of stabilized zirconia. The large volume of research has been driven by the use of stabilized zirconia as a solid electrolyte in high temperature electrochemical devices such as oxygen sensors and solid oxide fuel cells (SOFC). These applications use rapid oxygen ion diffusion, with oxygen ions being the fastest diffusing species in the fluorite crystal lattice. Much of the early research on stabilized zirconia compared materials prepared by different methods,

* Corresponding author. Department of Chemical Engineering and Materials Science, 916 Engineering Tower, Irvine, CA 92697-2575, USA. Tel.: +1-949-824-2919; fax: +1-949-824-2541.
E-mail address: martham@uci.edu (M.L. Mecartney).

0167-2738/03/$ - see front matter © 2003 Elsevier B.V. All rights reserved.
doi:10.1016/S0167-2738(03)00265-0

processed with different heat treatments and with different grain sizes. However, one common theme that emerged was the recognition that grain boundaries in stabilized zirconia act as barriers to oxygen ion conductivity [2–19].

Increased resistance to ionic transport across the grain boundaries (relative to the grain interior) is known as the grain boundary blocking effect. Impedance spectroscopy can provide information on the grain interior (bulk) conductivity, σ_{interior}, and the total grain boundary conductivity, $\sigma_{\text{Total gb}}$, and the overall total conductivity of the samples (grain interiors + grain boundaries). Impurities at grain boundaries contribute to grain boundary blocking, yet even in high purity 8 mol% yttrium cubic stabilized zirconia (Y-CSZ), the grain boundary specific conductivity is more than two orders of magnitude less conductive than the grain interior [3,4]. Thus the higher the volume fraction of grain boundaries in a sample (the smaller the grain size), the lower the total conductivity. Guo [5] and Guo and Maier [6] point out that this intrinsic grain boundary resistance in high purity materials may be a result of space charge oxygen vacancy depletion rather than contamination. Since the grain boundary can be considered to consist of two space charge layers separated by a grain boundary core, oxygen vacancy depletion in the space charge layer could be the cause of this grain boundary blocking effect [5–8]. Yttrium segregation, with the yttrium concentration at the grain boundary approximately twice as high as in the grain interior, is also present at Y-CSZ grain boundaries and through defect to defect interaction could provide a mechanism for localized oxygen vacancy depletion and/or vacancy trapping [9–14].

SiO_2 is generally considered a contaminant in Y-CSZ when used as a solid oxide electrolyte and it is believed to reduce the grain boundary ionic conductivity [3,4,7,15–19]. There has been much discussion as to whether a contaminating siliceous glassy phase [20] that segregates to the grain boundary covers the grains completely [21], partially [22] or not at all [3]. High resolution analytical TEM analyses, however, show SiO_2 segregation at three and four grain junctions but only segregation of Si^{4+} ions and not a discrete SiO_2 layer along two-grain boundaries [23].

Although silica is considered a detriment to ionic conducting materials, it can be an aid to sintering, densification and superplastic deformation. Efforts to minimize the deleterious effects of SiO_2 in Y-CSZ include adding Al_2O_3, which has been shown to increase ionic conductivity by scavenging of silica contamination [16,17,24–26]. However, Badwal et al. [27] have recently determined that the addition of alumina considerably degrades conductivity in very "pure" materials. Heat treatments have also been used to improve grain boundary conductivity of Y-CSZ containing a siliceous phase (precursor scavenging) [19]. However, inherent in many of these techniques to enhance conductivity is intrinsic grain growth and the concomitant grain boundary volume fraction reduction.

Superplastic deformation of Y-CSZ has been demonstrated to be possible by adding a few weight percent of silica [28]. The silica segregates to the multiple grain junctions in Y-CSZ and pins the grains via Zener pinning [29] and limits the rapid grain growth that normally prevents superplastic deformation [28]. Electrolyte design is currently limited to simple shapes due to the manufacturing cost associated with any shape not easily extruded or cast. Complex shapes with a higher efficiency might be achievable if they could be net shape formed using superplastic deformation. However, quantitative data that correlates conductivity with grain size as a function of silica content is required to assess the viability of using silica as a grain pinning second phase in electrolytes. This paper provides that data and addresses the separate roles of grain boundary segregation and grain size on grain boundary conductivity and total ionic conductivity for Y-CSZ.

2. Experimental

2.1. Sample preparation

Commercially available high purity 8 mol% Y-CSZ powder (Tosoh, Japan) with a crystallite size of 25 nm was used to prepare samples with no additives (hereafter called "pure" samples) and samples with 1 wt.% (2.5 vol.%), 3 wt.% (7.5 vol.%), 5 wt.% (12.5 vol.%) and 10 wt.% (25 vol.%) colloidal silica (Nissan Chemicals, New York) with a particle size of 12–14 nm. High purity Tosoh Y-CSZ is produced by a hydrolysis process and contains 20–40 ppm silica. Slurries were

prepared with Y-CSZ, colloidal silica and isopropanol. Slurries were mixed by attritor-milling in a medium of yttrium-containing tetragonal zirconia polycrystal (Y-TZP) balls for 4 h and allowed to air dry. This was followed by an overnight vacuum bake at 120 °C. The resultant cake was crushed back to powder and sieved to <80 μm. The sieved powder was cold isostatically pressed for 5 min at 55 kpsi to fabricate circular cylinders in 1.0×1.5 cm molds.

For this study, all samples were sintered at 1350 °C for 0.1 h except for a control group of "pure" Y-CSZ samples annealed without sintering. (This control group gave indistinguishable impedance results from the sintered samples for the same anneal condition.) The temperature ramp rate was 10 °C/min for heating and samples were furnace cooled in air.

After sintering, the circular cylinders were sliced into disks 1–3 mm thick. Heat treatment consisted of annealing at selected times and temperatures from 0.5 to 100 h at 1500–1600 °C in air. The anneal temperature ramp rate was 20 °C/min for heating and power off furnace cooling.

2.2. Density, SEM, XRD and EDS

Green densities were calculated geometrically. Densities of the annealed samples were measured by the Archimedes method with water unless samples were not dense enough to have closed porosity, in which case volume and weight measurements were used to calculate density. A theoretical density of 5.96 g/cm^3 was used for pure Y-CSZ. The theoretical densities of samples containing silica were calculated by using the rule of mixtures.

Scanning electron microscopy (Philips XL 30 FEG) was used to obtain photomicrographs from polished surfaces after thermal etching at 1300 °C for 30 min. The grain boundaries were outlined using image analysis software (Scion Image) and the measured values for grain size were multiplied by 1.74 to obtain a "true" grain size [30]. The grain areas determined this way compared favorably with the standard line intercept method [31] and had the advantage of being more consistent.

X-ray diffraction (XRD) analysis was conducted with a Siemens X-ray Diffraktometer D5000 equipped with a graphite monochromator using Cu Kα ($\lambda =$ 0.15406 nm) radiation to verify phase and composition. Scans consisted of 0.02° steps for 2 s from 18° to 38°.

An EmiSPEC Vision integrated acquisition system interfaced to a Philips CM200-FEG with an Oxford super-ATW detector and XP3 pulse processor was used to acquire EDS spectrum lines (typically 20 points, 0.5–2.0 nm spacing, 10 s dwell/point, ~1.25 nA beam current, 1.2 nm spot size) across edge-on grain boundaries and across grain boundary triple points at Oak Ridge National Laboratory. Spectra were "post-processed" interactively with the Vision software to yield profiles of background-subtracted integrated intensities.

2.3. Impedance spectroscopy

Samples for conductivity studies were polished with 600-grit silicon carbide paper. Samples previously polished to ~1 μm for grain size analysis were roughed up with 600-grit abrasive to enhance electrode adhesion. Porous platinum paste electrodes were applied (Gwent Electronic Material, UK) to the surface and fired for 30 min at 1300 °C. The samples were sandwiched between two platinum plates in a spring-loaded alumina fixture that positioned the sample in the center of a Lynburg furnace with an alumina tube. Twenty-gauge platinum wires (~16 in.) connect the platinum plates to BNC connectors on the bulkhead of the alumina fixture. A K-type thermocouple temperature probe was placed through the bulkhead to monitor the temperature next to the sample.

Impedance spectra were obtained (HP 4192A LF Impedance Analyzer, Hewlett Packard, Palo Alto, CA) in air, at seven frequencies per decade over a frequency range of 5 Hz–13 MHz at temperatures of 350, 400, 450, 500, 550, 600 700 and 400 °C. The second 400 °C "cool down" measurement served to insure reproducibility. The temperature ramp rate was 10 °C/min with a 30-min dwell at each temperature for stability prior to data measurement. To reduce noise, a four-wire measurement technique was used with the common ground at the sample fixture bulkhead. The sample voltage was 0.3 V. The test fixture and test set up were calibrated and adjusted for inductance at frequencies over 500 kHz. Repeatability was determined to be furnace limited to 6% by performing multiple tests of several pure Y-CSZ samples.

3. Results

3.1. Microstructure

Table 1 shows that the initial heat treatment at 1350 °C generally produced fully dense samples. However, the pure Y-CSZ sample that was sintered at 0.1 h at 1350 °C and received no additional heat treatment had a relative density of only 83%. The addition of as little as 1 wt.% silica was sufficient enhancement for the calculated density to reach >99% even for samples sintered only at 1350 °C for 0.1 h. Larger amounts of silica were a detriment to densification when annealed a long time at higher temperature, since samples with 5% and 10% silica added and annealed for 100 h at 1600 °C had less than 95% relative density. Microcracks and fractures were observed on both of these samples. These microcracks were of limited depth, but present throughout the samples. Given the reduction in relative density of the samples at either extreme in heat treatment, the sample set reported here brackets the useful available grain sizes for study.

As shown in Table 2, grain size varied with heat treatment and the amount of silica added. The grain size consistently increased with additional heat treatment for a given silica content. The grain sizes in the pure Y-CSZ samples varied from 0.65 to 28.6 μm. The grain size consistently decreased as the silica content increased for a given heat treatment. This grain pinning effect due to intergranular silica is shown in Fig. 1, where the grain size decreased from 4.5 to 0.9 μm as the silica content increased from 0 to 10 wt.%. The contact between the grains appears to reduce as the silica content increases. At 10 wt.% silica, there appears to be very little contact between the grains. By controlling the amount of grain boundary pinning second phase and the heat treatment, a predetermined grain size may be engineered. As the heat treatment time or temperature increased, some grains in the SiO_2-doped materials exhibited abnormal grain growth relative to the average grain size, most likely due to inhomogeneous distribution of silica. This bimodal grain size distribution is less evident with increasing amounts of silica. X-ray diffraction analysis did not show the presence of any additional phases such as $ZrSiO_4$.

Table 1
Relative density

	0.1 h, 1350 °C	0.5 h, 1500 °C	2 h, 1500 °C	2 h, 1600 °C	100 h, 1600 °C
Y-CSZ	83%	96%	99%	100%	100%
1% SiO_2	99%	100%	100%	100%	99%
3% SiO_2	100%	100%	100%	99%	98%
5% SiO_2	100%	100%	100%	94%	91%
10% SiO_2	100%	100%	99%	97%	94%

Table 2
Grain size (μm)

	0.1 h, 1350 °C	0.5 h, 1500 °C	2 h, 1500 °C	2 h, 1600 °C	100 h, 1600 °C
Y-CSZ	0.65	3.1	4.5	10.2	28.6
1% SiO_2	0.62	1.3	1.6	2.8	21
3% SiO_2	0.51	1.1	1.5	1.7	10
5% SiO_2	0.46	1.0	1.2	1.6	6.7
10% SiO_2	0.31	0.75	0.9	1.2	4.0

3.2. Electrical

The raw impedance data was normalized for sample geometry to allow direct resistivity plotting. Fig. 2 is an example of Y-CSZ analyzed at different temperatures with two well-defined arcs, representing the grain interior resistivity and the total grain boundary contribution to resistivity. The total resistivity is the sum of the two arcs. Using the ratio of the arcs' maxima and the grain size allows the calculation of the specific grain boundary conductivity and the grain boundary width by the "brick layer" model [1,6,32–34]. The specific grain boundary conductivity is the average conductivity of the grain boundary and is equal to:

$$\sigma_{\text{sp. gb}} = (\delta/d)\sigma_{\text{Total gb}} \quad (1)$$

where δ is the grain boundary width and d is the grain size. The grain interior and grain boundary data were plotted as conductivity as shown in Fig. 3, by analyzing the temperature (T) dependence of the ionic conductivity (σ) per the Arrhenius equation:

$$\sigma = (A/T)\exp(-Q/kT) \quad (2)$$

where k is the Boltzmann constant and Q the activation energy. The temperature range for the impedance

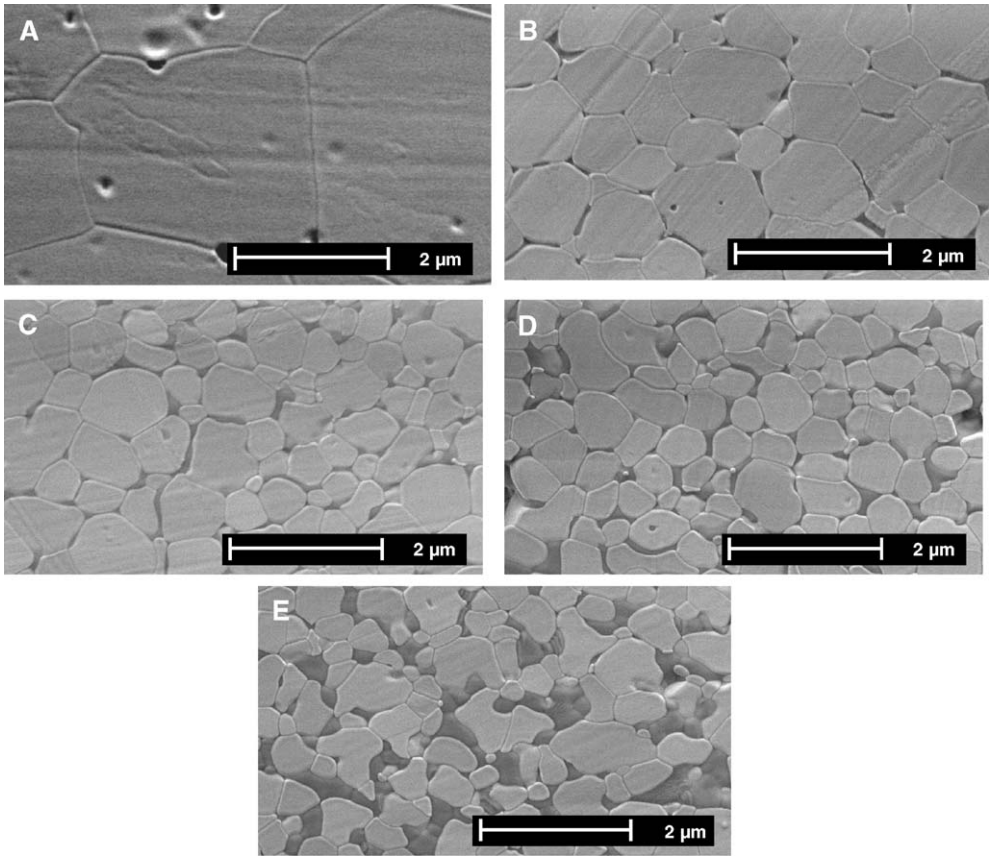

Fig. 1. Grain pinning with increasing weight percent of silica in Y-CSZ annealed at 1600 °C for 2 h. (A) 0 wt.% SiO_2, (B) 1 wt.% SiO_2, (C) 3 wt.% SiO_2, (D) 5 wt.% SiO_2 and (E) 10 wt.% SiO_2.

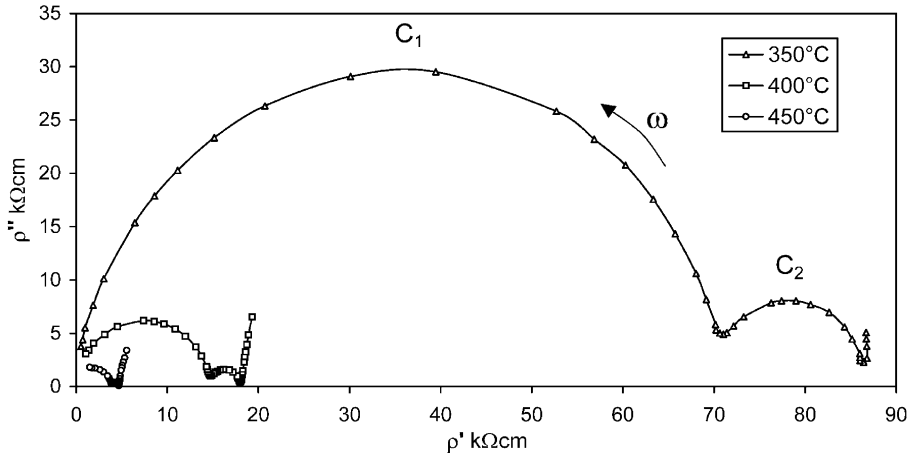

Fig. 2. Resistivity of Y-CSZ decreases rapidly with increasing temperature.

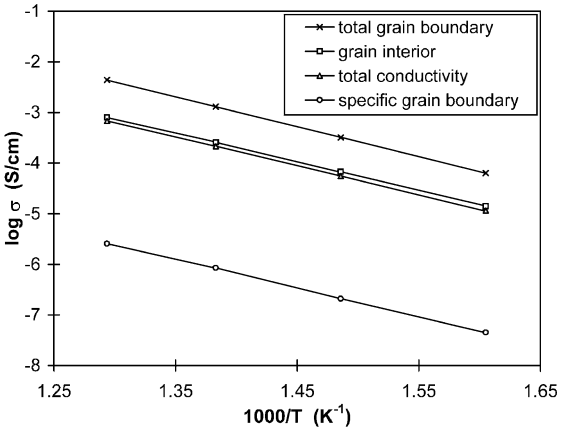

Fig. 3. Ionic conductivity of pure Y-CSZ heat-treated for 2 h at 1500 °C.

spectroscopy data presented was limited to 500 °C because the two arcs are not well defined above 500 °C.

The specific grain boundary conductivities were typically more than two orders of magnitude smaller than the grain interior bulk conductivity, even for the very pure material (Fig. 3). By definition, the activation energy for conduction is proportional to the Arrhenius slope. The activation energies for the grain interior and the grain boundaries are tabulated in Table 3. Within the error bar bracketed by the temperature stability of the furnace, the samples had a fairly narrow range of Q from 1.0 to 1.2 eV for both grain boundary and bulk, with and without silica, and at different grain sizes. The average activation energy for the grain boundary was approximately 5% higher than the activation energy for the grain interior.

The effect of the heat treatment on grain interior conductivity and specific grain boundary conductivity was analyzed by plotting the conductivities of the

Table 3
Activation energy (eV) of grain interior/grain boundary

	0.1 h, 1350 °C	0.5 h, 1500 °C	2 h, 1500 °C	2 h, 1600 °C	100 h, 1600 °C
Y-CSZ	1.14/1.15	1.17/1.22	1.12/1.12	1.13/1.11	1.11/1.25
1% SiO_2	1.01/1.05	1.08/1.14	1.11/1.17	1.10/1.16	1.09/1.16
3% SiO_2	1.08/1.14	1.12/1.18	1.12/1.09	1.08/1.13	1.12/1.18
5% SiO_2	1.11/1.20	1.12/1.17	1.12/1.17	1.13/1.20	1.14/1.15
10% SiO_2	1.12/1.21	1.10/1.16	1.13/1.19	1.11/1.18	1.11/1.16

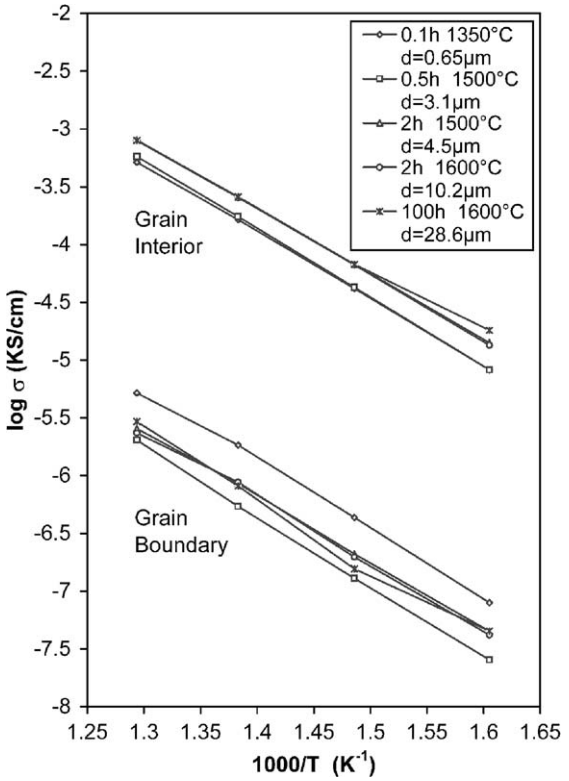

Fig. 4. Conductivity of grain interior and specific grain boundary of pure Y-CSZ with different heat treatments/grain sizes.

grain interior and the specific grain boundary (Fig. 4 for Y-CSZ without SiO_2). As expected, except for the highly porous samples, the measured conductivity of the grain interior did not change significantly with heat treatment [35]. This was also true for heat treatments of samples with the same amount of second phase silica (Fig. 5). However, samples with increasing amounts of silica receiving the same heat treatment consistently showed a slight reduction in grain interior conductivity. The reduction of grain interior conductivity with SiO_2 addition shown in Fig. 6 was typical for any given heat treatment. With increasing addition of silica from 1 to 10 wt.%, the grain interior conductivity as determined by the brick layer model decreased by approximately 25%. The total grain boundary conductivity decreased with increasing SiO_2 due to the increase in grain boundary volume fraction. This effect is responsible for the increased size of the second arc (total grain boundary resistivity) in Fig. 6A.

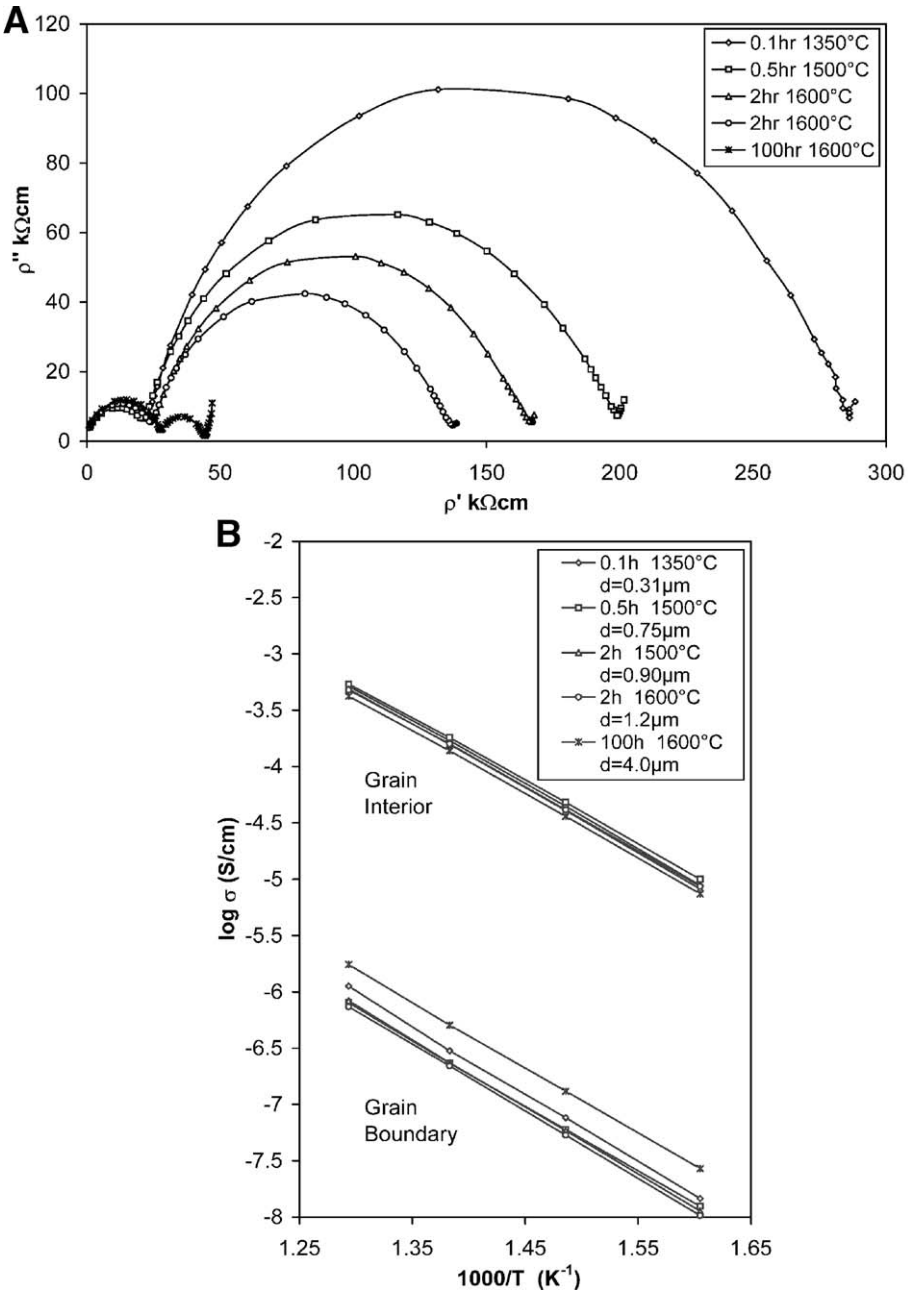

Fig. 5. Y-CSZ with 10 wt.% SiO_2 at different heat treatments/grain sizes. (A) Impedance spectroscopy data at 400 °C. (B) Grain interior and specific grain boundary conductivity.

The specific grain boundary conductivity for all samples was consistently about two orders of magnitude lower than the bulk conductivity (Figs. 4 and 5). For a given amount of silica added, the specific grain boundary conductivity was tightly grouped irrespective of heat treatment (except for the porous samples). As shown in Fig. 6, the grain boundary specific conductivity appeared to consistently decrease with

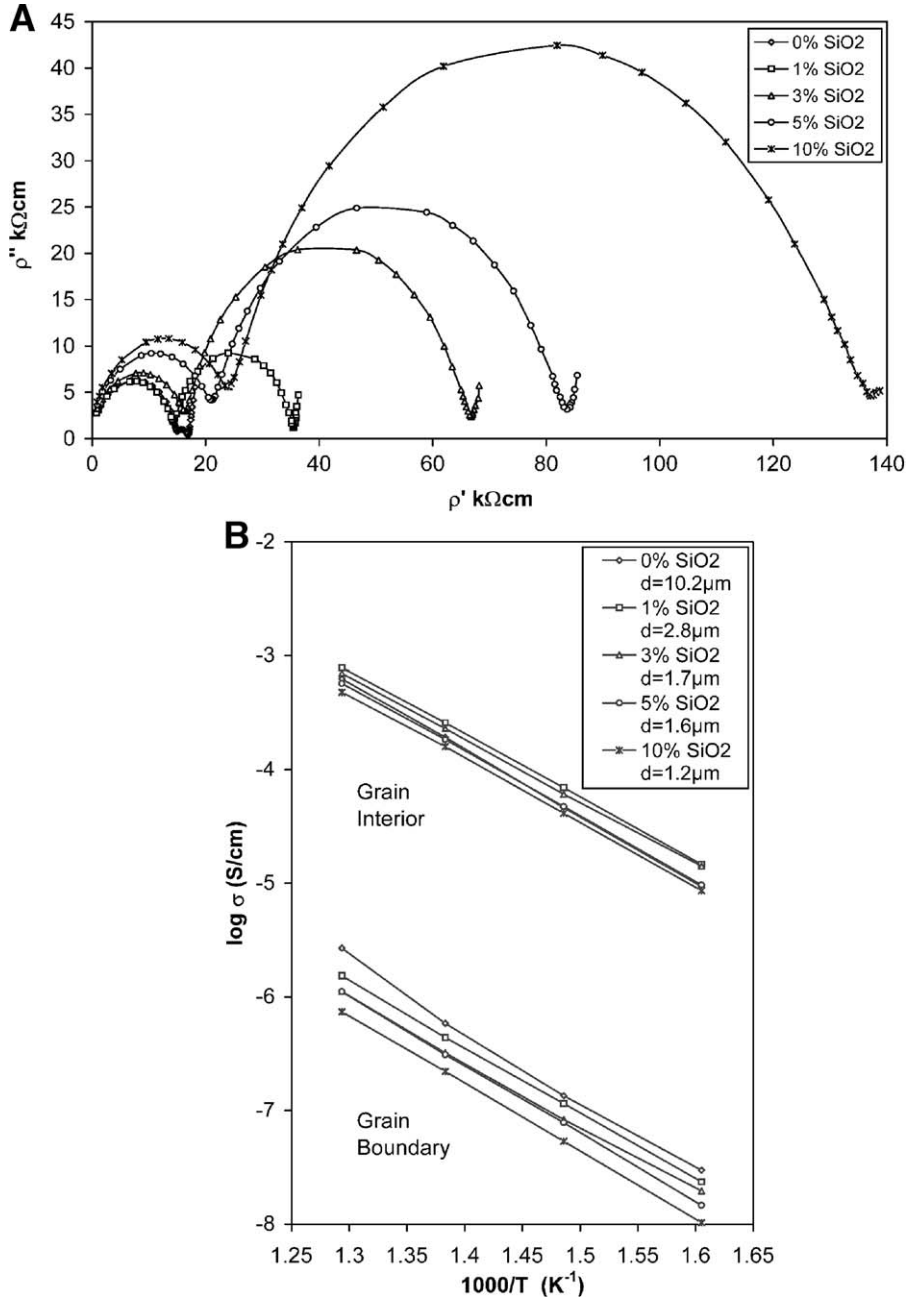

Fig. 6. Y-CSZ with different amounts of silica added annealed for two h at 1600 °C. (A) Impedance spectroscopy data at 400 °C. (B) Grain interior and specific grain boundary conductivity.

the addition of silica. However, although silica adversely affected grain boundary conductivity, it did not appear to be as significant as previously thought where researchers reported greater than an order of magnitude reduction in conductivity for even very small amounts of silica [3,4,7,15–19,36,37]. The pertinent

figure of merit for solid oxide electrolytes is the total conductivity, which can be increased by a heat treatment that increases the grain size. To properly judge the impact of added silica to total conductivity, samples with a similar grain size should be analyzed so that grain boundary area is consistent. This can be done by comparing samples with the same grain size and different amounts of silica.

The conductivities of samples with the same grain size after heat treatment are shown in Fig. 7. Samples with a grain size of 1.2 μm (Fig. 7a) showed the total conductivity and specific grain boundary conductivity for 1 and 5 wt.% silica were the same, while the conductivities of the 10 wt.% silica sample were half of that. Samples with a consistent grain size of 3 or 10 μm (Fig. 7b and d) showed no difference in total or specific grain boundary conductivity between pure Y-CSZ and 1 wt.% silica added (Fig. 7b) or between pure Y-CSZ and 3 wt.% silica added (Fig. 7d). Samples with a 4-μm grain size (Fig. 7c) confirm,

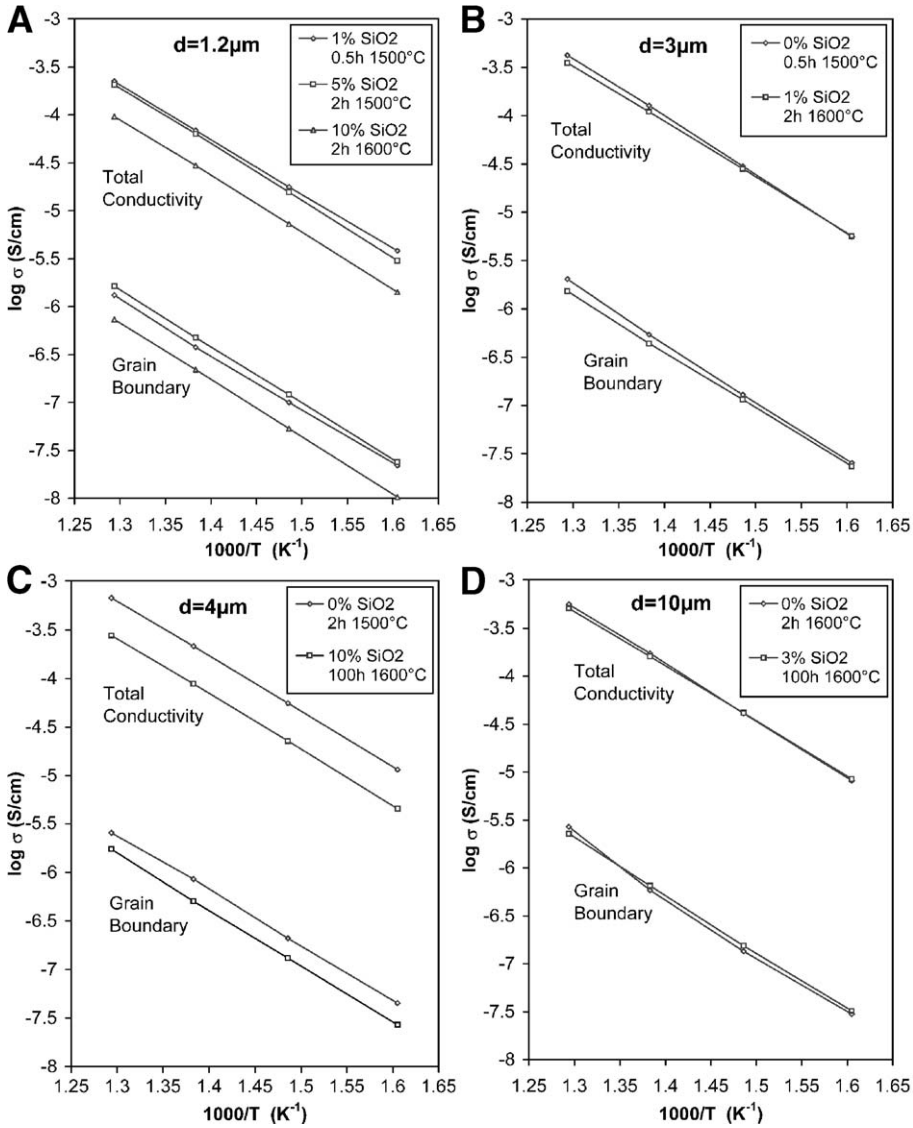

Fig. 7. Conductivity data for samples with a constant grain size. (A) $d = 1.2$ μm, (B) $d = 3$ μm, (C) $d = 4$ μm and (D) $d = 10$ μm.

Table 4
Grain boundary width (nm)

	0.1 h, 1350 °C	0.5 h, 1500 °C	2 h, 1500 °C	2 h, 1600 °C	100 h, 1600 °C
Y-CSZ	6.1	4.0	2.9	3.9	4.5
1% SiO_2	4.1	5.4	5.4	6.8	11.0
3% SiO_2	4.3	6.9	6.6	7.0	8.2
5% SiO_2	5.2	6.9	6.5	7.7	8.1
10% SiO_2	6.2	7.8	7.3	7.3	8.7

however, that the presence of 10 wt.% silica reduces the conductivity.

The grain boundary width (δ), tabulated in Table 4 was calculated from impedance data

$$\delta = d(C_1/C_2)(\varepsilon_{gb}/\varepsilon_{interior}) \quad (3)$$

and showed values ranging from 3 to 11 nm. It was assumed that $\varepsilon_{gb} \sim \varepsilon_{interior}$. In general, the grain boundary width increased with both heat treatment and the addition of silica.

4. Discussion

Data gathered in this study correlate well with published values for conductivity. For example, the bulk conductivity measured value of 4.5 mS/cm for Y-CSZ at 600 °C is consistent with the 4–5 mS/cm values reported by others [1,3,4,35]. The grain boundary specific conductivity is 100–1000 times less than the bulk conductivity, which agrees with previous measurements [4]. The total grain boundary conductivity represented by the second impedance spectroscopy arc increases with grain size, d, but the grain boundary specific conductivity does not increase with grain size [2,4]. The values of activation energy in the range of 1.0–1.2 eV are in agreement with the 1.1 eV generally reported for Y-CSZ [1,3,4,35]. On average, the specific grain boundary activation energy is larger than the grain interior activation energy by approximately 5%, which is consistent with the 5–10% difference reported by others [4,5,35].

The calculated grain boundary widths in Table 4 presume a similarity of permittivity between the grain boundary and the grain interior (Eq. (3)). If $\varepsilon_{gb} < \varepsilon_{interior}$ for samples containing silica, then the calculated value of grain boundary width would be decreased. The values of grain boundary width measured by impedance spectroscopy ranged from 3 to 11 nm. These dimensions, however, do approximate the grain boundary widths obtained from preliminary analytical TEM analyses (Fig. 8) for a typical Y-CSZ sample with 1 wt.% SiO_2. The grain boundary width values are close to the 5–8 nm reported for Y-TZP with added silica [14], but are larger than values of 2 nm reported for pure 10Y-CSZ [35].

Much of the previous discussion in the literature has centered on the continuity of the boundary film and the coverage of the siliceous phase. Given the very low solubility of silica in zirconia [38], it is apparent that as the grains grew, the silica phase remained segregated. Although some silicon ions remain segregated at two-grain boundaries along with yttrium and zirconium ions, the excess SiO_2 is forced to the triple points and there is no continuous discrete grain boundary film. This concept is supported by the similarity in grain boundary specific conductivity with or without silica added (Fig. 7). If a discrete SiO_2 layer existed (contrary to high resolution analytical TEM [14]), the

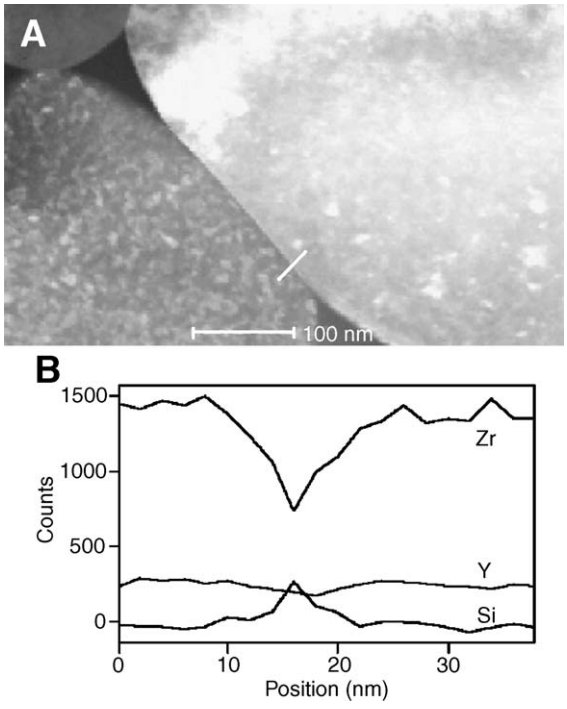

Fig. 8. TEM EDS analysis of grain boundary composition for Y-CSZ with 1 wt.% of SiO_2. (A) Twenty-point line scan with 1.2 nm probe across grain boundary. (B) Grain boundary composition.

measured grain boundary conductivity would have been much lower than for pure samples. The two orders of magnitude reduction in grain boundary conductivity compared to the grain interior in even very pure material was likely caused by a combination of space charge layer oxygen depletion and yttria segregation induced local lattice disorder. Fig. 8 demonstrates that the ratio of Y/Zr is much higher at the grain boundaries than in the grain interior.

The apparent, albeit small, linear reduction of the bulk conductivity with larger additions of silica was harder to explain (Fig. 6). The volume fraction of intergranular phase in the sample may have played a role similar to porosity in decreasing the effective measurement of true grain interior conductivity for larger volume fractions. The pure Y-CSZ sample sintered only at 1350 °C for 0.1 h had a grain interior conductivity very similar to the sample with 10 wt.% silica added and annealed for 100 h at 1600 °C and the volume fractions of Y-CSZ grains in these samples were both low (83% and 75%, respectively).

Previous research had suggested that the large reduction in the total ionic conductivity of Y-CSZ in the presence of SiO_2 was caused by the blocking effect of silica segregated to the grain boundary [3,4,7,15–19]. However, these results have not considered the smaller grain size that results from the retarding effect on grain growth of the silica second phase. Adding silica to very pure Y-CSZ lowered conductivity in at least four ways: (1) There was a slight reduction in the grain boundary specific conductivity. (2) The average grain boundary width, as determined by impedance spectroscopy, increased by as much as a factor of 2 with the addition of silica. (3) The volume of nonconductive phase increased, influencing bulk conductivity. (4) The grain boundary volume fraction increased because the grain size was much smaller. The increase in grain boundary volume fraction had by far the greatest impact on total conductivity. The grain boundary width increase and reduced grain boundary specific conductivity accounted for reducing the conductivity by about half. However, the effect of a reduced grain size and increased grain boundary volume fraction from grain boundary pinning accounted for over an order of magnitude reduction in conductivity. A heat treatment that reduces the grain boundary volume fraction by increasing the grain size can restore much of the total conductivity lost by adding silica, even though the volume fraction of the nonconducting phase remains the same (Fig. 7). This grain growth heat treatment would reduce the grain boundary volume fraction and force excess silica to the triple points.

The four charts of Fig. 7 clearly demonstrate the importance of the relationship of grain size to ionic conductivity. Adding silica to Y-CSZ pinned the grains, via Zener pinning [29], substantially reduced the grain size and increased the grain boundary volume fraction. Because the grain boundary was intrinsically 100 to 1000 times less conductive than the bulk, the smaller grain size resulted in lowered ionic conductivity. For larger grain sizes, the grain boundary volume fraction was lower and the conductivity was higher. Data show that for a *similar grain size*, less than 5 wt.% SiO_2 will not degrade either total conductivity or grain boundary specific conductivity (Fig. 7). However, the effect of SiO_2 on the oxygen exchange kinetics at the electrode/electrolyte interface have not been addressed.

This study has concentrated on the effects on and correlation of grain size to ionic conductivity. The role of grain boundary width has yet to be analyzed in similar fashion, but future research will focus on the use of high resolution analytical TEM to correlate chemical segregation with the grain boundary width determined by impedance spectroscopy. A more accurate determination of the grain boundary composition using analytical TEM will provide a better estimate of the grain boundary permittivity and a more accurate calculation of grain boundary width. Even though the grain boundary width would be smaller if $\varepsilon_{gb} < \varepsilon_{interior}$, and this would affect the calculation of specific grain boundary conductivity, the measurements presented here of total ionic conductivity (the most relevant parameter for applications) are not affected by the addition of less than 5 wt.% SiO_2 for samples with the same grain size (Fig. 7).

5. Conclusions

Adding a small amount of silica (< 5 wt.%) to Y-CSZ does not appreciably affect the grain boundary conductivity or the total conductivity when compared to "pure" Y-CSZ samples with a similar grain size. The addition of small amounts of silica "pins" the Y-CSZ grains during sintering and densification, limiting grain growth and dramatically increasing the grain

boundary volume. Since the grain boundary specific conductivity of even very pure material is two to three orders of magnitude lower than the grain interior conductivity, any increase in grain boundary volume will always decrease the total ionic conductivity for Y-CSZ. A heat treatment that reduces the grain boundary volume fraction by increasing the grain size restores much of the conductivity lost by adding silica. For Y-CSZ samples with less than 5 wt.% SiO_2, the grain boundary specific conductivity and the total conductivity are similar to samples of Y-CSZ with a similar grain size. Heat treatments may be used to engineer a larger grain size, lower grain boundary volume and improve total electrolyte conductivity. This would be important for applications using superplastic deformation where an initial small grain size is required. Parts could be shape formed while the grains are small and then an appropriate anneal could be used to grow the grains and improve conductivity.

Acknowledgements

The authors very much appreciate the following assistance: Sossina Haile of California Institute of Technology for help with the impedance spectroscopy test set and test result data discussions; Arthur Nowick of the University of California, Irvine, for helpful discussions and review of this manuscript; Mike Ing of the University of California, Irvine, for help with test set construction and sample preparation; Kathryn Hedges of the University of California, Irvine, for editorial support; Phil Imamura of the University of California, Irvine, and Neal Evans of the Oak Ridge National Laboratory for TEM EDS data gathered under SHaRE program contract no. DE-AC05-76OR00033; National Science Foundation for support under grant DMR-0207197; and additional financial support from the National Fuel Cell Research Center at UC Irvine. The detailed comments from *Solid State Ionics* reviewers.

References

[1] J.E. Bauerle, Journal of Physics and Chemistry of Solids 30 (1969) 2657.
[2] A.I. Ioffe, M.V. Inozemtsev, A.S. Lipilin, M.V. Perfilev, S.V. Karpachov, Physica Status Solidi. A 30 (1975) 87.
[3] M. Aoki, Y.-M. Chiang, I. Kosacki, L.J.R. Lee, H. Tuller, L. Yaping, Journal of the American Ceramic Society 79 (1996) 1169.
[4] M.J. Verkerk, B.J. Middelhuis, A.J. Burggraaf, Solid State Ionics 6 (1982) 159.
[5] X. Guo, Solid State Ionics 81 (1995) 235.
[6] X. Guo, J. Maier, Journal of the Electrochemical Society 148 (2001) E121.
[7] M.J. Verkerk, A.J.A. Winnubst, A.J. Burggraaf, Journal of Materials Science 17 (1982) 3113.
[8] S.H. Chu, M.A. Seitz, Journal of Solid State Chemistry 23 (1978) 297.
[9] A.P. Santos, R.Z. Domingues, M. Kleitz, Journal of the European Ceramic Society 18 (1998) 1571.
[10] E.C. Dickey, F. Xudong, S.J. Pennycook, Journal of the American Ceramic Society 84 (2001) 1361.
[11] S. Stemmer, J. Vleugels, O. Van Der Biest, Journal of the European Ceramic Society 18 (1998) 1565.
[12] M.M.R. Boutz, C. Chu Sheng, L. Winnubst, A.J. Burggraaf, Journal of the American Ceramic Society 77 (1994) 2632.
[13] S.-L. Hwang, I.-W. Chen, Journal of the American Ceramic Society 73 (1990) 3269.
[14] Y. Ikuhara, P. Thavorniti, T. Sakuma, Acta Materialia 45 (1997) 5275.
[15] M. Godickemeier, B. Michel, A. Orliukas, P. Bohac, K. Sasaki, L. Gauckler, H. Heinrich, P. Schwander, G. Kostorz, H. Hofmann, O. Frei, Journal of Materials Research 9 (1994) 1228.
[16] A.J. Feighery, J.T.S. Irvine, Solid State Ionics 121 (1999) 209.
[17] E.P. Butler, J. Drennan, Journal of the American Ceramic Society 65 (1982) 474.
[18] C.C. Appel, N. Bonanos, Journal of the European Ceramic Society 19 (1999) 847.
[19] J.-H. Lee, T. Mori, L. Ji-Guang, T. Ikegami, M. Komatsu, H. Haneda, Journal of the Electrochemical Society 147 (2000) 2822.
[20] M.L. Mecartney, Journal of the American Ceramic Society 70 (1987) 54.
[21] M. Ruhle, N. Claussen, A.H. Heuer, in: N. Claussen, M. Ruhle (Eds.), Advances in Ceramics, The American Ceramic Society, Columbus, Ohio, 1988, p. 352.
[22] T. Stoto, M. Nauer, C. Carry, Journal of the American Ceramic Society 74 (1991) 2615.
[23] Y. Ikuhara, Y. Nagai, T. Yamamoto, T. Sakuma, Towards Innovation in Superplasticity II, Transtec Publications, Zurich-Uetikon, 1999, p. 525.
[24] S. Rajendran, J. Drennan, S.P.S. Badwal, Journal of Materials Science Letters 6 (1987) 1431.
[25] X. Guo, Y. Runzhang, Journal of Materials Science 30 (1995) 923.
[26] Y. Ji, J. Liu, Z. Lu, X. Zhao, T. He, W. Su, Solid State Ionics 126 (1999) 277–283.
[27] S.P.S. Badwal, F.T. Ciacchi, V. Zelizko, Ionics 4 (1998) 25.
[28] A.A. Sharif, M.L. Mecartney, Acta Materialia 51 (2003) 1633.
[29] C.S. Smith, Transactions of the American Institute of Mining and Metallurgical Engineers 175 (1948) 15.
[30] A.W. Thompson, Metallography 5 (1972) 366.

[31] M.I. Mendelson, Journal of the American Ceramic Society 52 (1969) 443.
[32] S.M. Haile, D.L. West, J. Campbell, Journal of Materials Research 13 (1998) 1576.
[33] H. Nafe, Solid State Ionics 13 (1984) 255.
[34] J.R. MacDonald, Impedance Spectroscopy: Emphasizing Solid Materials and Systems, Wiley-Interscience, New York, 1987.
[35] S.P.S. Badwal, J. Drennan, Journal of Materials Science 22 (1987) 3231.
[36] S.P.S. Badwal, S. Rajendran, Solid State Ionics 70 (1994) 83.
[37] J.-H. Lee, T. Mori, J.G. Li, T. Ikegami, M. Komatsu, H. Haneda, Journal of the American Ceramic Society 83 (2000) 1273.
[38] W.C. Butterman, W.R. Foster, in: H.M. Ondik, H.F. McMurdie (Eds.), Phase Diagrams for Zirconium and Zirconia Systems, The American Ceramic Society, Westerville, OH, 1998, p. 134.